

# Vibration energy harvesting using piezoelectric unimorph cantilevers with unequal piezoelectric and nonpiezoelectric lengths

Xiaotong Gao,<sup>1</sup> Wei-Heng Shih,<sup>1,a)</sup> and Wan Y. Shih<sup>2</sup>

<sup>1</sup>Department of Materials Science and Engineering, Drexel University, Philadelphia, Pennsylvania 19104, USA

<sup>2</sup>School of Biomedical Engineering, Science and Health Systems, Drexel University, Philadelphia, Pennsylvania 19104, USA

(Received 22 March 2010; accepted 16 October 2010; published online 6 December 2010)

We have examined a piezoelectric unimorph cantilever (PUC) with unequal piezoelectric and nonpiezoelectric lengths for vibration energy harvesting theoretically by extending the analysis of a PUC with equal piezoelectric and nonpiezoelectric lengths. The theoretical approach was validated by experiments. A case study showed that for a fixed vibration frequency, the maximum open-circuit induced voltage which was important for charge storage for later use occurred with a PUC that had a nonpiezoelectric-to-piezoelectric length ratio greater than unity, whereas the maximum power when the PUC was connected to a resistor for immediate power consumption occurred at a unity nonpiezoelectric-to-piezoelectric length ratio. © 2010 American Institute of Physics.

[doi:10.1063/1.3521389]

Piezoelectric energy harvesting devices which offer the advantages of small size, high electromechanical coupling, and ease of miniaturization have been increasingly investigated as an enabling technology for self-powered systems such as wireless sensor networks.<sup>1-3</sup> In particular, piezoelectric unimorph cantilevers (PUCs) consisting of a piezoelectric layer bonded to a nonpiezoelectric layer have been one of the most studied piezoelectric vibration/impact energy harvesting devices.<sup>4-6</sup> So far most of PUC energy harvesters consist of a piezoelectric and a nonpiezoelectric layer that are of the same lengths. Gao *et al.*<sup>7</sup> studied PUCs with unequal piezoelectric and nonpiezoelectric lengths with a concentrated force applied at the tip and found that the PUC with a longer nonpiezoelectric layer gave a larger induced voltage. Furthermore, the induced voltage increased monotonically with an increasing nonpiezoelectric length. The situation of energy harvesting from a vibration source is of

both fundamental and practical importance. However, it is not clear whether the induced voltage simply increases monotonically with an increasing length ratio between the piezoelectric and nonpiezoelectric layers or there exists an optimal length ratio under dynamic loading. The purpose of this study is to examine the induced voltage as well as power of PUCs of unequal piezoelectric and nonpiezoelectric lengths under vibration of a given frequency.

A PUC with unequal piezoelectric and nonpiezoelectric lengths can be treated as a two-section beam: section-1, comprised of the piezoelectric layer, nonpiezoelectric layer and bonding layer, and section-2, comprised of either the nonpiezoelectric layer [Fig. 1(a)] or the piezoelectric layer [Fig. 1(b)]. Eurturk *et al.* proposed a differential equation that governs the deflection of a PUC with equal piezoelectric and nonpiezoelectric lengths.<sup>8</sup> This differential equation can be generalized to apply to a two-section PUC as

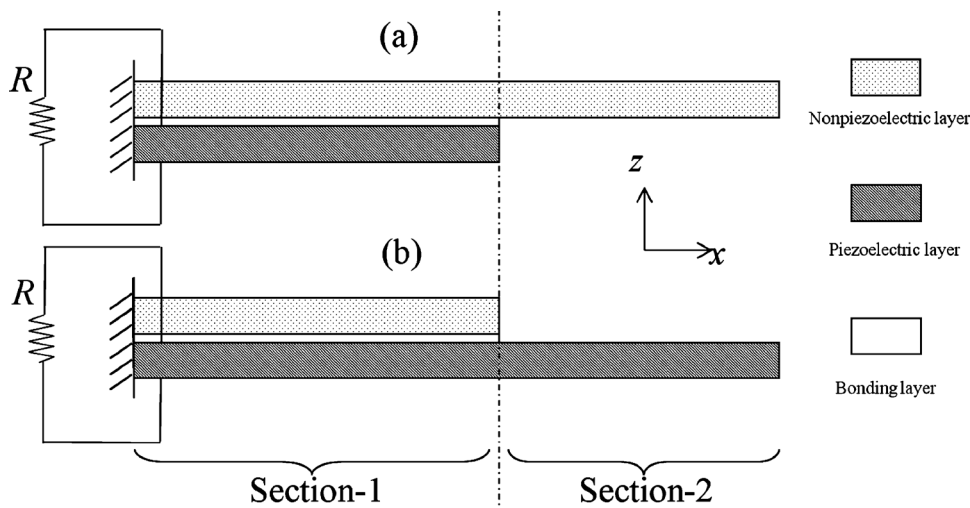


FIG. 1. Schematics of PUCs with (a) a longer nonpiezoelectric layer and (b) a longer piezoelectric layer.

<sup>a)</sup>Electronic mail: shihwh@drexel.edu

$$D_i \frac{\partial^4 w_{rel,i}(x,t)}{\partial x^4} + c_{s,i} I_i \frac{\partial^5 w_{rel,i}(x,t)}{\partial x^4 \partial t} + c_a \frac{\partial w_{rel,i}(x,t)}{\partial t} + m_i \frac{\partial^2 w_{rel,i}(x,t)}{\partial t^2} + \vartheta_i v(t) \left[ \frac{d\delta(x-x_{1,i})}{dx} - \frac{d\delta(x-x_{2,i})}{dx} \right] = -m_i \frac{\partial^2 w_b(x,t)}{\partial t^2} - c_a \frac{\partial w_b(x,t)}{\partial t}, \quad (1)$$

where subscripts  $i=1$  and  $2$  stand for section-1 and section-2, respectively,  $w_{rel,i}(x,t)$  denotes the cantilever deflection relative to the base motion,  $D_i$  denotes the bending modulus,  $c_{s,i}$  denotes the equivalent strain rate damping coefficient,  $I_i$  denotes the area moment of inertia of the cross section,  $m_i$  denotes the mass per unit length,  $\vartheta_i$  denotes a piezoelectric coupling term,<sup>8</sup>  $c_a$  denotes the viscous air damping coefficient,  $v(t)$  denotes the voltage across the piezoelectric layer,  $\delta(x)$  denotes the Dirac delta function, and  $x_{1,i}$  and  $x_{2,i}$  denote the boundaries of the electrodes on the piezoelectric layer with  $x_1 < x < x_2$  and  $w_b(x,t)$  denotes the base motion. The relative deflection of section- $i$  in a freely vibrating two-section PUC can be expressed as<sup>9</sup>

$$w_{rel,i}(x,t) = \sum_{r=1}^{\infty} h_{i,r}(x) \eta_r(t), \quad (2)$$

where  $h_{i,r}(x)$  and  $\eta_r(t)$  are the eigenfunction and the time-dependent function of the  $r$ th mode vibration, respectively. The expressions for  $h_{i,r}(x)$  and the resonant frequency of the two-section PUC were obtained using the transcendental-equation procedure described by Shen *et al.*<sup>10</sup> Substituting Eq. (2) into Eq. (1) and following the procedure in Ref. 8, the expressions of  $w_{rel,i}$ , induced voltage, current, and power were obtained. The details of the procedure will be published subsequently.

Experimentally, PUCs comprised of a 127  $\mu\text{m}$  thick lead zirconate titanate (PZT) layer (PSI-5H4E, Piezo Systems, Inc., Woburn, MA) bonded to a 50  $\mu\text{m}$  thick stainless steel (SS) layer were fabricated. The length of the PZT layer in all the PUCs was 39.5 mm while the length of the SS layer was varied from 10 to 70 mm. The widths of all the PUCs were 5.5 mm. The average thickness of the epoxy bonding layer was 40  $\mu\text{m}$ . For power generation, the PZT was connected to a resistor as shown in Fig. 1. The PUCs were vibrated at their first-mode resonant frequencies by using a mechanical shaker. The induced voltage across the PZT layer was measured by using an oscilloscope. The tip displacement of the PUCs and the base vibration amplitude,  $A_b$ , were measured by using a laser displacement meter. The base acceleration amplitude,  $a_b$ , was obtained from  $a_b = A_b \omega_b^2$ , where  $\omega_b$  is the angular frequency of the base vibration. In the calculation, instead of theoretically evaluating the strain rate damping and viscous air damping coefficients, the mechanical damping ratios of the PUCs measured by using the logarithmic decrement method<sup>11</sup> under short-circuit (SC) condition were used.<sup>8</sup> The capacitances of the PZT layers were also measured and used in the calculation. Since the PUCs were vibrated at their first-mode resonant frequencies, the contributions from higher modes were neglected. In the following, the resonant frequency refers to the first-mode resonant frequency unless otherwise indicated.

In Fig. 2(a), the SC resonant frequencies of the PUCs were plotted versus the SS/PZT length ratio,  $\Phi$ , which shows

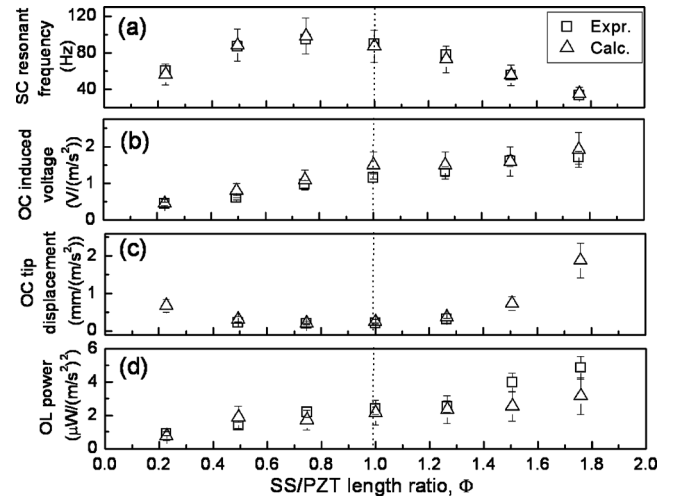


FIG. 2. (a) SC resonant frequency, (b) OC induced voltage, (c) OC tip displacement, and (d) power with an optimal resistive load (OL) of PUCs with different SS/PZT length ratios,  $\Phi$ . The vertical dashed line indicates the unity  $\Phi$ .

that the calculated values were consistent with the experimental results. It is interesting to note that a maximum resonant frequency occurred at  $\Phi \approx 0.75$ . The induced voltage amplitude and tip displacement amplitude normalized by the base acceleration amplitude at open-circuit (OC) condition were shown in Figs. 2(b) and 2(c), respectively. As can be seen, the experiments and the calculations were in good agreement and the induced voltage increased with an increasing  $\Phi$ . In Fig. 2(c), we missed some of the tip displacement data as they were out of the range of the laser displacement meter. The error bars of the calculations were estimated from the tolerances of the material properties provided by the manufacturers. In Fig. 2(d), the power consumed by an optimal resistive load, which matched the impedance of the PUC, was plotted versus  $\Phi$ . Note that the optimal load resistances of the PUCs were not necessarily the same as the resonant frequencies and damping ratios of the PUCs were different.<sup>12</sup> As can be seen in Fig. 2(d), the experiments and calculations were in good agreement and the power increased with an increasing  $\Phi$ . The experimental results validated the above described analytical approach toward a two-section PUC.

Using the validated analytical approach, a case study was carried out to compare the induced voltage and power of PUCs of different  $\Phi$  for a presumed fixed base vibration frequency of 90 Hz. All PUCs had the same PZT and epoxy thicknesses of 127 and 40  $\mu\text{m}$ , respectively, and the same width of 5.5 mm while different SS thicknesses (50, 100, and 200  $\mu\text{m}$ ) were examined. For a PUC of a given PZT length, the SS length was chosen such that the OC resonant frequency,  $f_{OC}$ , of the PUC matched the base vibration frequency, 90 Hz. A mechanical damping ratio of 0.9%, based on the average of the measured damping ratios of the PUCs in the above experiments was used. In Fig. 3(a), the PZT and SS lengths of PUCs with  $f_{OC}=90$  Hz were plotted versus  $\Phi$ . As can be seen, for a given SS thickness, there was a finite range of PZT and SS lengths that can result in an  $f_{OC}$  of 90 Hz. If the PZT length was greater than a certain value (42, 48, and 57.9 mm for 50, 100, and 200  $\mu\text{m}$  thick SS, respectively), no SS length could be adjusted to give an  $f_{OC}$  of 90 Hz. Similarly, if the SS length was greater than a certain

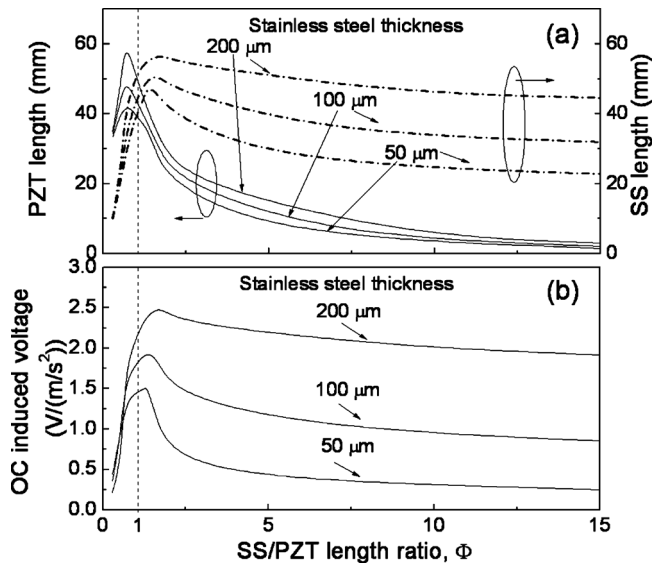


FIG. 3. Calculated (a) PZT and SS lengths as a function of the SS/PZT length ratio,  $\Phi$ , for PUCs with an  $f_{OC}$  of 90 Hz and (b) the corresponding open-circuit (OC) induced voltage under 90 Hz base vibration. The vertical dashed line indicates the unity  $\Phi$ .

value (47.1, 50.7, and 56.4 mm for 50, 100, and 200  $\mu\text{m}$  thick SS, respectively), no PZT length could be adjusted to give an  $f_{OC}$  of 90 Hz. In Fig. 3(b), one can see that the OC induced voltage peaked at  $\Phi > 1$  for all SS thicknesses. This is because, as shown in Fig. 3(a), when  $\Phi$  increases from unity, the SS layer as well as the entire PUC is getting longer. As a result, the PUC becomes more flexible for deflection which tends to generate a larger induced voltage under the same vibration. On the other hand, the smaller PZT length associated with a larger  $\Phi$  reduces the length of section-1, thus increases the stiffness and decreases the deflection and induced voltage in section-1. These two competing effects, the decrease of the stiffness of the entire PUC and the increase of the stiffness of section-1, result in the optimal  $\Phi$  in Fig. 3(b). For a PUC with  $\Phi < 1$ , section-2 is comprised solely of the PZT layer [Fig. 1(b)] which produces no net induced charges as the strain neutral axis in section-2 is located at the midpoint of the thickness of the PZT layer. Such an “inactive” portion of the PZT layer decreases the overall induced voltage.<sup>7</sup> Furthermore, the induced voltage was also affected by the thickness of the SS layer. As shown in Fig. 3(b), for the same  $\Phi$ , the OC induced voltage increased with the SS thickness. This was because, with a thicker SS layer, the PZT layer was farther away from the strain neutral axis and therefore a larger average strain can be generated within the PZT layer.<sup>8</sup> The optimal  $\Phi$  also increased with an increasing SS thickness: 1.28, 1.45, and 1.71 for 50, 100, and 200  $\mu\text{m}$  thick SS, respectively. In addition, the enhancement in terms of the OC induced voltage at the optimal  $\Phi$  compared to that at  $\Phi = 1$  also increased with an increasing SS thickness: 4.6%, 8.4%, and 16.9% for 50, 100, and 200  $\mu\text{m}$  thick SS, respectively.

The power dissipated over a resistive load connected to the PUCs was also examined at 90 Hz. The optimal load resistance,  $R_{opt}$ , of the PUCs was plotted as a function of  $\Phi$  in Fig. 4(a) together with the corresponding induced voltage,  $V_{in}$ . The behavior of  $V_{in}$  was found to be similar to the OC

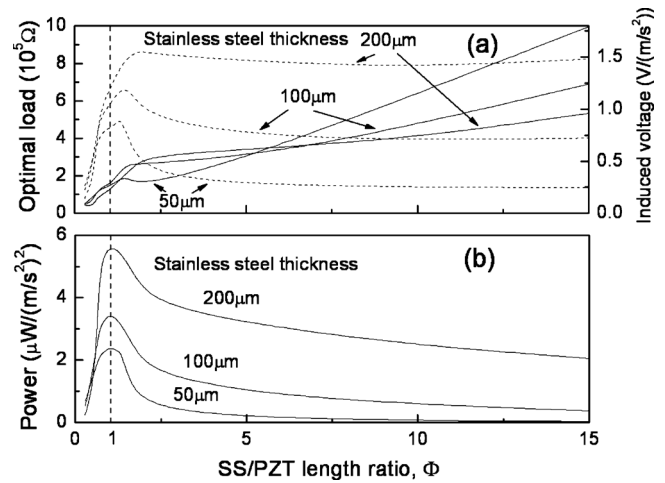


FIG. 4. Calculated (a) induced voltage (dashed curve) and optimal load resistance (solid curve) and (b) power output as a function of SS/PZT length ratio,  $\Phi$ . The vertical dashed line indicates the unity  $\Phi$ .

induced voltage in Fig. 3(b). The  $V_{in}$  peaked not at  $\Phi = 1$  but at an optimal  $\Phi$  which was greater than unity. Both the optimal  $\Phi$  and the enhancement of  $V_{in}$  increased with an increasing SS thickness. However, the maximum power, which is determined by  $V_{in}^2/2R_{opt}$ , peaked at  $\Phi = 1$  as shown in Fig. 4(b). The different behaviors of the  $V_{in}$  and power are due to the dependence of  $R_{opt}$  on  $\Phi$  as shown in Fig. 4(a). Thus, for applications that require a high  $V_{in}$ , the optimal  $\Phi$  should be chosen whereas a unity  $\Phi$  should be used when a high power is required. An  $\Phi$  between unity and the optimal value may be chosen to obtain both appropriate  $V_{in}$  and power.

The present work showed that the maximum OC induced voltage which is important for capacitor or battery charging for later use occurred with a PUC that had a nonpiezoelectric-to-piezoelectric length ratio greater than unity. On the other hand, the maximum power, when the PUC is connected to a resistor for immediate power consumption, occurred at a unity nonpiezoelectric-to-piezoelectric length ratio.

This work is supported in part by the National Institute of Health (NIH) Grant No. 1 R01 EB000720 and the Nanotechnology Institute, a University Grant program of the Commonwealth of Pennsylvania's Ben Franklin Technology Development Authority through Ben Franklin Technology Partners of Southeast Pennsylvania.

- <sup>1</sup>C. B. Williams and R. B. Yates, *Sens. Actuators, A* **52**, 8 (1996).
- <sup>2</sup>S. Roundy, P. K. Wright, and J. Rabaey, *Comput. Commun.* **26**, 1131 (2003).
- <sup>3</sup>J. A. Paradiso and T. Starner, *IEEE Pervasive Comput.* **4**, 18 (2005).
- <sup>4</sup>S. Priya, *J. Electroceram.* **19**, 165 (2007).
- <sup>5</sup>S. R. Anton and H. A. Sodano, *Smart Mater. Struct.* **16**, R1 (2007).
- <sup>6</sup>H. Sodano, D. J. Inman, and G. Park, *Shock Vib. Dig.* **36**, 197 (2004).
- <sup>7</sup>X. Gao, W.-H. Shih, and W. Y. Shih, *Smart Mater. Struct.* **18**, 125018 (2009).
- <sup>8</sup>A. Erturk and D. J. Inman, *Trans. ASME, J. Vib. Acoust.* **130**, 041002 (2008).
- <sup>9</sup>L. Meirovitch, *Fundamentals of Vibrations* (McGraw-Hill, Boston, 2001).
- <sup>10</sup>Z. Y. Shen, W. Y. Shih, and W.-H. Shih, *Rev. Sci. Instrum.* **77**, 065101 (2006).
- <sup>11</sup>C. F. Beards, *Structural Vibration: Analysis and Damping* (Arnold, London, 1996).
- <sup>12</sup>Y. B. Liao and H. A. Sodano, *Smart Mater. Struct.* **18**, 045011 (2009).